AIAA 2002-2872

HIGH-ORDER MODELING OF MICRO-PULSED PLASMA THRUSTERS

Guang Lin and George Em Karniadakis*
Division of Applied Mathematics
Brown University
Providence, RI 02912

ABSTRACT

We present a new approach to model micro-pulsed plasma thrusters (micro-PPTs) as a single-fluid/two-temperature plasma flow, coupled with the external circuit of the triggering mechanism and with Teflon ablation. The plasma flow is rarefied as the typical Knudsen number is above 0.1. We adopt a continuum-based methodology that treats the viscous effects and employs the Navier-Stokes equations modified at the wall surface with appropriate velocity-slip and temperature-jump boundary conditions. A method is also introduced that guarantees pressure positivity even for very large density jumps that are typical in micro-PPTs. A spectral/hp element spatial discretization is employed on both structured and unstructured meshes. It is based on a discontinuous Galerkin treatment of the advection and diffusion components. Simulations of one-, two- and three-dimensional fully coupled micro-PPT flows are presented.

*Corresponding author, gk@cfm.brown.edu

INTRODUCTION

The increasing importance of micro-propulsion has led to systematic investigations of Pulsed Plasma Thruster (PPT) behavior, higher efficiency and better performance [1, 2, 3, 4]. The micro-Pulsed Plasma Thruster (micro-PPT) is a simplified version of the PPT designed primarily for propulsion and positioning of micro-satellites.

The micro-PPT has inherited some design characteristics from the standard PPT. However, the electronics is the main difference between the micro-PPT and the standard PPT. The micro-PPT only uses one circuit and one DC-DC converter. Work under development by the U.S. AFOSR, e.g. [5], has considered two main classes of micro-PPT electronic designs. One is the triggered micro-PPT and the other is the self-triggering micro-PPT. The self-triggering micro-PPT is designed to be simpler and much lighter than the triggered one. A micro-PPT's typical size is of the order of 1mm, which is one order of magnitude less than the standard PPT design. The typical energy discharge is of the order of 1 J, and the ablated material per pulse is about 1 μg.

Modeling of thrusters in micro-domain requires a new approach to treat the viscous effects and there may be an overlap of electro-dynamic and gas dynamics scales. A combined atomistic-continuum approach is required to address issues associated with non-equilibrium effects, especially for the very small micro-PPT designs. In particular, in addition to the multi-species nature of the flow in PPTs and the coupling with the external circuit and the ablating solid surface, in micro-PPTs we also need to address:

- Continuum and transitional rarefied regimes.
- Multiple time and length scales.
- Viscous layers and sheath interactions.
- Local non-equilibrium effects.
- Different electric circuits.
- New self-triggering mechanisms.

Neglecting the inertia contribution from the electrons and considering that ions and electrons have different temperatures, we model micro-PPTs as a single-fluid/two-temperature flow, coupled with the external circuit of the triggering mechanism and with Teflon ablation. The imposition of the divergence-free condition for the magnetic field results in a loss of the hyperbolicity of the ideal MHD equations. The development of suitable Riemann solvers for this case by Powell [6] can be easily extended to multi-dimensions and also to high-order discretization [7].

The compressible single-fluid/two-temperature MHD equations are strongly coupled and exhibit mixed hyperbolic/parabolic character depending on the parameter range. Most of these issues have been addressed in the published works [6, 7, 8, 9, 10, 11]. However, one of the limitations of the current numerical simulations is that they are of low-order accuracy. High-order methods are more suitable for resolving small scales and capturing the inherent transient behavior in the viscous micro-pulsed plasma thrusters. To solve the MHD system with high-order accuracy, a spectral/hp element spatial discretization is employed based on both structured and unstructured meshes. The discontinuous Galerkin treatment is applied to both the advection and diffusion components; more details can be found in [12].

The plasma flow is rarefied as the typical Knudsen number is above 0.1. A high-order boundary condition for velocity-slip and temperature-jump developed in [13] has been implemented in the context of the continuum approach. To decrease the discretization errors and guarantee *pressure positivity* even for large density jumps that are typical in micro-PPTs, a numerical strategy presented in [14] is incorporated.

In the following, we first introduce the algorithm for the 1D fully coupled micro-PPT system. Then, we discuss issues associated with rarefaction effects and how to modify the wall surface with appropriate velocity-slip and temperature-jump conditions. Subsequently, we present the method to maintain pressure positivity. We then present numerical simulations of MHD flow in micro-PPT in two- and three dimensions. Finally, we conclude with a brief summary.

1D FULLY COUPLED MHD SYSTEM

The main idea in the algorithm to model the 1D fully coupled micro-PPT is that the solutions obtained from the external circuit and ablation model will be used as the time-dependent boundary condition for solving the 1D MHD system. In the following, we present the main steps of the proposed algorithm.

Let us assume that all functions at the n-th time level are known, namely: ρ^n, u^n, B^n, I^n, q_c^n, E_{ind}^n, R_p^n. The numerical algorithm will then compute these functions at the next (n+1)-th time level, in six sub-steps.

- 1^{st} *step: Compute current/charge in circuit*

$$L_o\frac{d^2q_c}{dt^2} + (R_o + R_p)\frac{dq_c}{dt} + E_{ind} + \frac{q_c}{C} = 0 \quad (1)$$

for which the following initial conditions are used:

$$t = 0 : q(t=0) = \frac{V_o}{C}, \frac{dq}{dt} = 0, E_{ind} = 0, R_p = 0 \quad (2)$$

where L_o is the inductivity of the external circuit,

q_c is the charge on the capacitor,

C is the capacity of the capacitor,

R_o is the resistance of the external circuit,

R_p is the plasma resistance.

- 2^{nd} *step: Compute external electric field*

$$V_{PPT}^{n+1} = E_{ind}^n - I^{n+1}R_p^n \quad (3)$$

and

$$E_{ext}^{n+1} = \frac{V_{PPT}^{n+1}}{h} \quad (4)$$

where E_{ind} is the *emf*, induced by the plasma-dynamic processes in the PPT channel,

I is the total electrical current in the circuit,

V_{PPT} is the voltage drop on the PPT electrodes.

E_{ext} is the external electric field,

h is the distance between electrodes.

- 3^{rd} *step: Based on*

$$\widetilde{j}^{n+1} = \sigma^n(E_{ext}^{n+1} + E_{int}^n - u^n B^n) \quad (5)$$

where σ is the electrical conductivity,

B is the inductance of the magnetic field,

μ_o is the magnetic permeability, $\mu_o = 4\pi \cdot 10^{-7} H/m$,

We compute

$$B(x=0,t) = \frac{\mu_o \widetilde{j}^{n+1}}{W} \quad (6)$$

Then, we solve the 1D MHD system:

$$\frac{\partial \rho}{\partial t} + \frac{\rho u}{\partial x} = 0 \quad (7)$$

$$\frac{\partial \rho u}{\partial t} + \frac{\partial}{\partial x}(\rho u u + p) = \frac{\partial \tau_{xx}}{\partial x} + \widetilde{j} B \quad (8)$$

$$\frac{\partial}{\partial t}(\rho e_t) + \frac{\partial}{\partial x}[\rho u(e_t + \frac{p}{\rho})] = \frac{\partial}{\partial x}(\lambda \frac{\partial T}{\partial x}) + \frac{\partial}{\partial x}(u\tau_{xx}) + \frac{\widetilde{j}^2}{\sigma} \quad (9)$$

$$\frac{\partial B}{\partial t} + \frac{\partial}{\partial x}(uB) = \frac{\partial}{\partial x}[\frac{1}{\mu_o \sigma}\frac{\partial B}{\partial x}] \quad (10)$$

where λ is the thermal conductivity coefficient.

This solution will determine the following functions: ρ^{n+1}, u^{n+1}, B^{n+1}, e_t^{n+1}. Also, using e_t^{n+1} we can calculate the temperature T^{n+1}.

- 4^{th} *step: Determine total current and internal electric field*

$$j_{tot}^{n+1} = -\frac{1}{\mu_o}\frac{\partial B^{n+1}}{\partial x} \quad (11)$$

$$E_{int}^{n+1} = [\frac{j^{n+1}}{\sigma^{n+1}} - E_{ext}^{n+1} + u^{n+1}B^{n+1}] = [-\frac{1}{\mu_o \sigma^{n+1}}\frac{\partial B^{n+1}}{\partial x} - E_{ext}^{n+1} + u^{n+1}B^{n+1}] \quad (12)$$

where j_{tot} is the total current and E_{int} is the internal electric field.

- 5^{th} *step: Compute the induced emf electric field*

$$E_{ind}^{n+1} = R_p^{n+1} w \frac{B^{n+1}(x=0) - B^{n+1}(x=l)}{\mu_o} - w\frac{V_{PPT}^{n+1}}{h} + R_p^{n+1} w \int_{x=0}^{x=l} \sigma^{n+1} u^{n+1} B^{n+1} dx \quad (13)$$

where

$$R_p^{n+1} = \frac{1}{\int_{x=0}^{x=l} \sigma^{n+1} dx} \quad (14)$$

h is the height of the thruster,

w is the width of the thruster.

- 6^{th} *step: Compute heat flux for ablation model*

The heat flux to the PPT propellant Teflon surface:

$$q_w^{n+1} = -\lambda^{n+1}\frac{\partial T^{n+1}}{\partial x}|_{x=0} \quad (15)$$

$$T^{n+1}(x=0,t) = T_o + 2\frac{\widetilde{q}_w^{n+1}}{\lambda}\sqrt{\frac{\lambda t}{\pi \rho c}} \quad (16)$$

where

$$\widetilde{q}_w^{n+1} = q_w^{n+1} - [Q_{abl} + c(T_w - T_o)]G_w(T_w) \quad (17)$$

and the ablating gas flux is:

$$G_w^{n+1}(T_w) = (\rho u)_w^{n+1} = \frac{p_c^*}{\sqrt{\frac{m_{abl}}{2\pi k T_g}}} exp(\frac{-T_c^*}{T_w^{n+1}}), \quad (18)$$

Here, Q_{abl} is the ablation heat of Teflon, T_o is the temperature in-depth of the non-heated Teflon, k is the Boltzmann constant, T_g, T_w are the gas and surface temperature, and p_c^* and T_c^* are the empirical constants for Teflon ablation. In this case we assume that molecules C_2F_4 are the products of the vaporization, therefore $m_{abl} = 100 \cdot 1.7 \cdot 10^{-27} kg/molecule$.

Also, $u^{n+1}(x=0,t)$ can be obtained from G_w:

$$u^{n+1}(x=0,t) = \frac{G_w}{\rho_w^{n+1}} \quad (19)$$

Thus, from the ablation model we can update:

$$T^{n+1}(x=0,t), u^{n+1}(x=0,t) \quad (20)$$

- 7^{th} *step: Return to the* 1^{st} *step, using the following definition:* $\rho^n = \rho^{n+1}$, $u^n = u^{n+1}$, $B^n = B^{n+1}$, $I^n = I^{n+1}$, $q_c^n = q_c^{n+1}$, $E_{ind}^n = E_{ind}^{n+1}$, $R_p^n = R_p^{n+1}$.

SLIP BOUNDARY CONDITION

Deviation from continuum hypothesis is characterized by the Knudsen number, which is the ratio of the mean-free-path of the molecules to a characteristic length scale. According to the Knudsen number the flow can be divided into various regimes: continuum, slip, transition and free-molecular flow regimes. As Knudsen number is larger than 0.1, the Navier-Stokes equations break-down and a second-order accurate slip boundary condition in Kn is employed. The velocity-slip boundary conditions can be obtained by an approximate analysis of the motion of a monatomic gas near an isothermal surface [13]. Using Taylor series expansion, the slip relation on the boundaries becomes:

$$U_s - U_w = \frac{2-\sigma_v}{\sigma_v}[\lambda(\frac{\partial U}{\partial n})_s + \frac{\lambda^2}{2}(\frac{\partial^2 U}{\partial n^2})_s + ...] \quad (21)$$

where U_w is the tangential velocity of the wall, U_s is the fluid velocity near the wall and σ_v is the tangential momentum accommodation coefficient.

By nondimensionizing using a reference length and velocity scale, we have:

$$U_s - U_w = \frac{2-\sigma_v}{\sigma_v}[Kn(\frac{\partial U}{\partial n})_s + \frac{Kn^2}{2}(\frac{\partial^2 U}{\partial n^2})_s + ...] \quad (22)$$

where the Knudsen number (Kn) can be defined in terms of Mach number and Reynolds number i.e.,

$$Kn = \sqrt{\frac{\pi\gamma}{2}}\frac{M}{Re} \quad (23)$$

The expansion above originally given in [15] is first-order in Kn. To develop slip boundary conditions accurate up to the second-order terms in Kn, we introduce a new slip boundary condition in a general form [13],

$$U_s - U_w = \frac{2-\sigma_v}{\sigma_v}\frac{Kn}{1-B(Kn)Kn}\frac{\partial U}{\partial n}, \quad (24)$$

where $B(Kn)$ is an empirical parameter to be determined. This is a Pade approximation of Pade equation (22).

In a similar way, we can also derive the temperature-jump boundary conditions. Therefore, the non-dimensional form of the boundary conditions are:

$$U_s - U_{wall} = \frac{2-\sigma_v}{\sigma_v}\frac{Kn}{1-bKn}\frac{\partial U_s}{\partial n} \quad (25)$$

$$T_s - T_{wall} = \frac{2-\sigma_T}{\sigma_T}\frac{2\gamma}{(\gamma+1)}\frac{Kn}{Pr}\frac{\partial T}{\partial n} \quad (26)$$

where $\frac{\partial T}{\partial s}$ is the tangential temperature variation along the channel surface and σ_T is the thermal accommodation coefficient. We have developed a *penalty method* to implement the velocity-slip boundary condition, as follows

$$M\frac{dU_N}{dt} = DU_N - \tau M_s(U_N - U_s), \quad (27)$$

where M is the mass matrix and M_s is the surface mass matrix. Here τ is the penalty parameter, which has value $\tau > 1000$ from accuracy and stability considerations.

MAINTAINING PRESSURE POSITIVITY

In solving the MHD system, the pressure is a derived variable. It can be derived by subtracting off the kinetic energy and magnetic energy from the total energy. However, in the micro-PPT simulations, the pressure can be several orders of magnitude smaller than either the kinetic energy or the magnetic energy. Thus, small discretization errors in the total energy can produce situations where the pressure might become negative. This leads to an unacceptable physical situation in the simulation of micro-PPT. As long as the regions in front of a magneto-sonic shock have positive pressure, negative pressures would not be produced in magneto-sonic shocks.

One numerical technique to deal with this problem was presented in [14]. It solves the *entropy equation* instead of solving the total energy equation. We adopt this approach in our formulation.

We model the micro-PPT as a compressible viscous single-fluid/two-temperature MHD flow. The governing equations can be expressed in conservative form:

$$\frac{\partial \rho}{\partial t} = -\nabla\cdot(\rho v) \quad (28)$$

$$\frac{\partial(\rho v)}{\partial t} = -\nabla\cdot(\rho v v^t - BB^t + (p+\frac{1}{2}|B|^2)I - \frac{1}{S_v}\tau) \quad (29)$$

$$\frac{\partial B}{\partial t} = -\nabla\times(B\times v + \frac{1}{S_r}\nabla\times B) \quad (30)$$

$$\begin{aligned}\frac{\partial E}{\partial t} = &-\nabla\cdot((E+p)v + (\frac{1}{2}|B|^2 I - BB^t)\cdot v \\ &-\frac{1}{S_v}v\cdot\tau + \frac{1}{S_r}(B\cdot\nabla B - \nabla(B\cdot B)) \\ &-\frac{1}{S_v Pr_e}\nabla T_e - \frac{1}{S_v Pr_i}\nabla T_i) + J\cdot E\end{aligned} \quad (31)$$

$$\frac{\partial E_e}{\partial t} = -\nabla \cdot (E_e v + P_e v) + v \cdot \nabla P_e$$
$$+\frac{1}{Sv_e}\tau_e \cdot \nabla v + \nabla \cdot (\frac{1}{S_v Pr_e}\nabla T_e) + J \cdot E + \phi \quad (32)$$

$$\nabla \cdot B = 0 \quad (33)$$

$$\tau = (\partial_j v_i + \partial_i v_j) - \frac{2}{3}\nabla \cdot v \delta_i j \quad (34)$$

where

$$Pr = \frac{C_p \mu}{\kappa}, S_v = \frac{\rho_o V_A L_o}{\mu} \quad (35)$$

To employ the method mentioned above, we replace equations (31) and (32) by the following two entropy equations:

$$\frac{\partial S_i}{\partial t} = -\nabla \cdot (S_i v) + \frac{1}{T_i S_i}\tau \nabla v$$
$$+\nabla \cdot (\frac{1}{T_i Sv_i Pr_i}\nabla T_i) + \frac{J \cdot E}{T_i} + \frac{\phi_i}{T_i} \quad (36)$$

$$\frac{\partial S_e}{\partial t} = -\nabla \cdot (S_e v) + \frac{1}{T_e S_e}\tau \nabla v$$
$$+\nabla \cdot (\frac{1}{T_e Sv_e Pr_e}\nabla T_e) + \frac{J \cdot E}{T_e} + \frac{\phi_e}{T_e} \quad (37)$$

where S_i is the ion entropy and S_e is the electron entropy.

In the regions where the pressure is large enough and there are magneto-sonic shocks around, we use the usual MHD equations in conservative form. On the other hand, if the pressure is a very small fraction of the total energy and there are no shocks in the regions, the above entropy equations are used. To identify the regions that the pressure is much smaller than the total energy, we use the *switch1* mentioned in [14]. Specifically the entropy equation will be switched on at the (i,j,k) point if

$$P_{i,j,k} < \alpha E_{i,j,k} \quad (38)$$

and it is switched off in all other situations. Here α is set to 0.05. There are also several other options for switches in [14].

Using *switch1*, we only try to correct the regions where the pressure might potentially become negative. Since the total energy equation is used in most of the domain and pressure is still derived from the subtraction of two large numbers, the accuracy of the pressure is not better than the overall accuracy.

Another important issue must be stressed here. In employing equations (36) and (37), we would have to give up conservation of energy. However, since equations (36) and (37) are only utilized in local regions of the flow, the conservation of total energy is violated only locally. Using such numerical strategy, we are able to reduce the discretization errors in the evaluation of the pressure and maintain positive pressure even for very large density jumps in the simulation of micro-PPTs.

NUMERICAL SIMULATION

1D fully coupled micro-PPT

First, we consider one-dimensional fully coupled MHD flows in LES/6 PPT. In the initial condition, we can see a steep density jump from $1.36 \times 10^{-2} kg/m^3$ to $1.36 \times 10^{-5} kg/m^3$. Figure 1 shows the compute domain. $x_o = 0m$ is the inlet of LES/6 PPT; $x_1 = 0.00245m$ is the location where the initial density has a large jump and the initial magnitude field reaches the maximum. $x_2 = 0.006m$ is the outlet of LES/6 PPT. $x_3 = 0.06m$ is the end of buffer. Figure 2 shows the coupled current waveform for the 1360V case. Figure 3 shows the corresponding voltage waveform. Figure 4 and figure 5 show the total resistance and the corresponding instantaneous power in total resistance.

Initial conditions

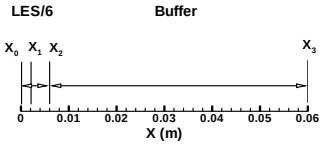

Figure 1: 1D LES/6 compute domain

$$x_0 \le x \le x_1 : \rho_1 = 1.36 \cdot 10^{-2} kg/m^3,$$
$$u_1 = 0, B_{1z} = \mu_o j_o x, T_1 = 10000K; \quad (39)$$

$$x_1 \le x \le x_2 :$$
$$\rho_2 = 1.36 \cdot 10^{-5} kg/m^3, u_2 = 0, \quad (40)$$
$$B_{2z} = 0.00245 \mu_o j_o \frac{0.006 - x}{0.006 - 0.00245}, T_2 = 10000K. \quad (41)$$

$$x_2 \le x \le x_3 : \rho_3 = 1.36 \cdot 10^{-5} kg/m^3,$$
$$u_3 = 0, B_{3z} = 0, T_3 = 10000K. \quad (42)$$

where:

$$\mu_o = 4\pi \times 10^{-7} \frac{H}{m}, \sigma_o = 1.32 \times 10^4 \frac{1}{\omega m}$$
$$V_o = 1360V,\ j_o = \sigma_o \frac{V_o}{h}, h = 0.03m$$

Boundary conditions

inflow:

$$x = x_0 : \rho = \rho_w, u = u_w, \frac{\partial B}{\partial x} = 0; \qquad (43)$$

outflow:

$$x = x_2 : \frac{\partial \rho}{\partial x} = \frac{\partial u}{\partial x} = \frac{\partial B}{\partial x} = 0. \qquad (44)$$

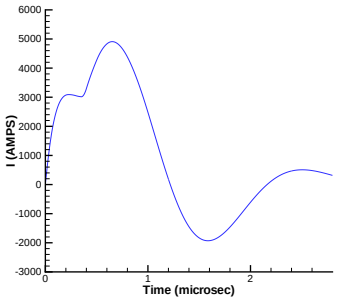

Figure 2: Current waveform for the 1360V case.

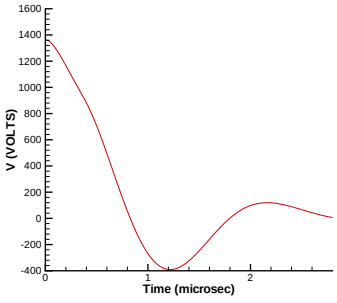

Figure 3: Voltage waveform.

Parametric Studies

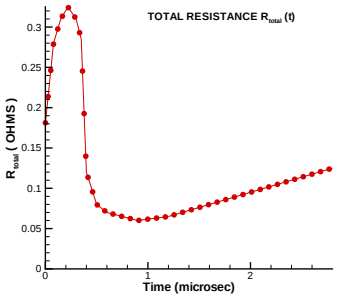

Figure 4: Total resistance $R_{total}(t)$.

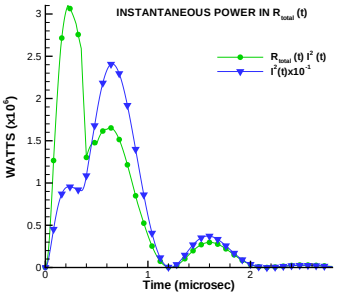

Figure 5: Instantaneous power in $R_{total}(t)$.

The ablation of Teflon determines the inlet velocity and the inlet temperature while the electric circuit determines the current waveform and corresponding magnetic field at the inlet. Therefore, these two thermal and electric domains are coupled to the MHD domain. We have studied how all these parameters affect the PPT acceleration and how to reach better design through parametric studies. Figure 6 shows the effects of initial magnetic field on streamwise velocity. The magnitude of streamwise velocity becomes larger and larger by increasing initial magnetic field. Figure 7 shows the effects of inlet velocity on streamwise velocity. The streamwise velocity waveforms are changed by increasing the magnitude of the inlet velocity. Figure 8 shows the effects of initial density jump on the streamwise velocity. The magnitude of streamwise velocity is increased by making the initial density jump larger. Figure 9 shows the effects of the current waveforms on the streamwise velocity. We can see the waveform of the streamwise velocity also can be changed by modifying the magnitude of the current waveforms.

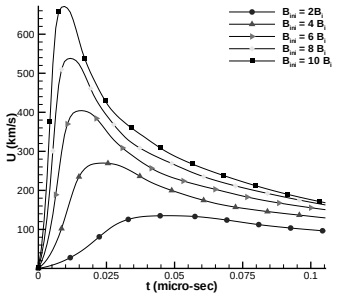

Figure 6: Effects of initial magnetic field on streamwise velocity.

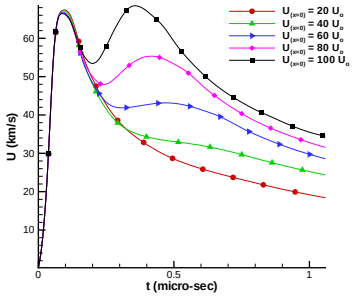

Figure 7: Effects of magnitude of inlet velocity on streamwise velocity.

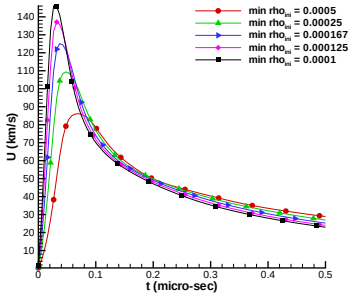

Figure 8: Effects of initial density jump on streamwise velocity.

Adaptive entropy fix

To decrease discretization errors and maintain pressure positive, only in the region that the pressure might become negative, we use the entropy equation, instead of the energy equation. Figures 10 shows the percentages of points solving the entropy equation with different density jumps. From this figure, we can see that more points are solved by the entropy equation, with larger density jump.

2D MHD flows in LES/6 PPT

Here we consider the LES/6 PPT geometry; see reference [16] for dimensions. The mesh we employed in the 2D simulations is shown in figure 11. In the initial condition (45), there is also a steep density jump from $1.36 \times 10^{-2} kg/m^3$ to $1.36 \times 10^{-5} kg/m^3$. The same numerical strategy as above is used in the simulation to maintain pres-

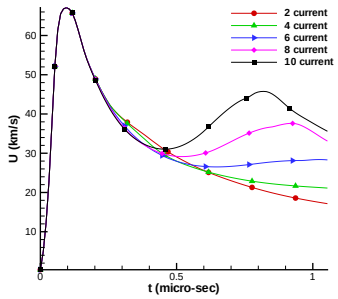

Figure 9: Effects of current waveforms on streamwise velocity.

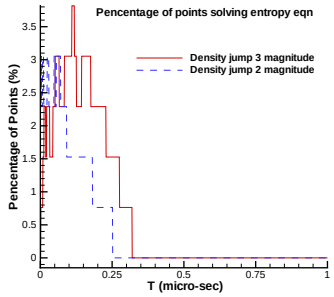

Figure 10: Percentages of points solving the entropy equation with different density jumps.

sure positivity.

Initial conditions

$$0 \le x \le 0.00245m : \rho_1 = 1.36 \cdot 10^{-2} kg/m^3,$$
$$u_1 = w_1 = 0, B_{1x} = 0, B_{1z} = \mu_o j_o x, T_1 = 10000K; \quad (45)$$

$$0.00245 \le x \le 0.006m :$$
$$\rho_2 = 1.36 \cdot 10^{-5} kg/m^3, u_2 = w_2 = 0, B_{2x} = 0, \quad (46)$$
$$B_{2z} = 0.00245 \mu_o j_o \frac{0.006 - x}{0.006 - 0.00245}, T_2 = 10000K. \quad (47)$$

$$0.006 \le x \le 0.06m : \rho_3 = 1.36 \cdot 10^{-5} kg/m^3,$$
$$u_3 = w_3 = 0, B_{3x} = 0, B_{3z} = 0, T_3 = 10000K. \quad (48)$$

where:
$\mu_o = 4\pi \times 10^{-7} \frac{H}{m}$,$\sigma_o = 1.32 \times 10^4 \frac{1}{\omega m}$
$V_o = 1360V$, $j_o = \sigma_o \frac{V_o}{h}$,$h = 0.03m$

Boundary conditions

Inflow (x=0 m):

$\rho = 1.36 \times 10^{-2} kg/m^3$
$B_x = 0(T), B_{z,inflow} = 0.001225 \mu_o j_o$

where:
$\mu_o = 4\pi \times 10^{-7} \frac{H}{m}, j_o = 5.984 \times 10^8 \frac{V}{\omega m^2}$
$T = 10000\kappa$
$u = U_s = \sqrt{\gamma RT}, w = 0$

Outflow (x=0.06 m):

$\rho = 1.36 \times 10^{-5} kg/m^3$
$B_x = 0(T), B_{z,outflow} = sB_{z,inflow} (s \le 0.1)$

$T = 10000\kappa$
$u = xU_s, (x > 1), w = 0$

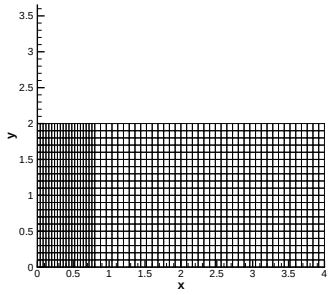

Figure 11: Structured mesh for two-dimensional PPT (LES/6) model.

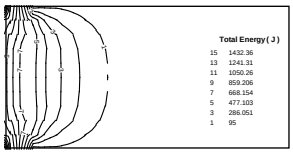

Figure 12: Total Energy at $0.2\mu - sec.$

We model micro-pulsed plasma thruster as a single-fluid/two-temperature plasma flow. That means the ion and the electron carry different temperatures. Figure 12 and figure 13 show the contours of the total energy and the electron energy.

Velocity-slip and temperature jump

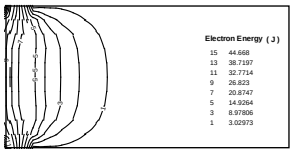

Figure 13: Electron Energy at $0.2\mu - sec$.

Figure 14 shows the corresponding Knudsen number at each point in micro-PPT and LES/6. The size of micro-PPT is $100\mu m$. We can see the Knudsen number in the micro-PPT is one order of magnitude larger than that in LES/6. Figure 15 shows the velocity profile using velocity slip condition.

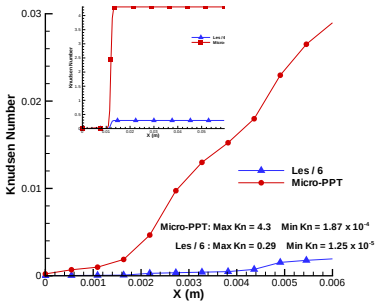

Figure 14: Knudsen number in micro-PPT and LES/6.

3D MHD flows in LES/6 PPT

Next we simulate the three-dimensional LES/6 PPT. The corresponding structured mesh is shown in figure 16. The initial and boundary conditions are similar to the two-dimensional case. There is also a steep density jump in the initial condition. In figures 17 and 18, we plot the instantaneous contours of the streamwise momentum at 0.2 and 0.4 $\mu - sec$ after start up.

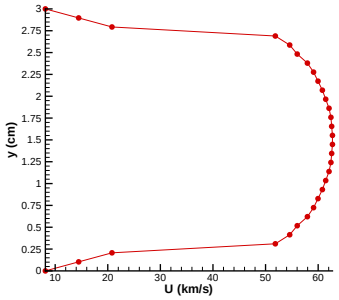

Figure 15: Velocity profile, using velocity-slip boundary conditions.

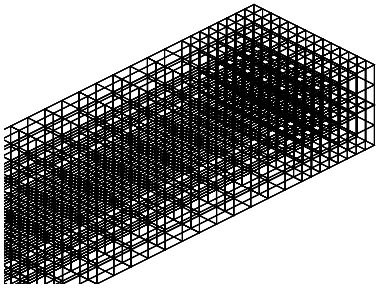

Figure 16: Structured mesh for three-dimensional PPT (LES/6) model.

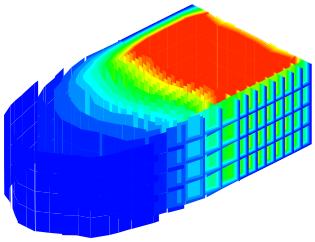

Figure 17: Streamwise momentum at 0.2 $\mu - sec$ in three-dimensional PPT (LES/6) model.

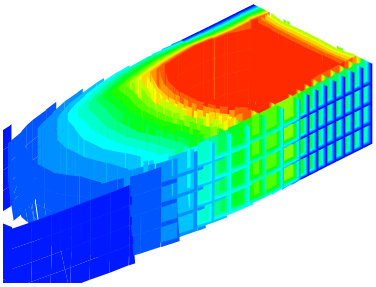

Figure 18: Streamwise momentum at $0.4\ \mu - sec$ in three-dimensional PPT (LES/6) model.

SUMMARY

The micro-PPT is modeled as a single-fluid/two-temperature plasma flow. Analysis of 1D fully coupled MHD model has indicated how the external circuit and Teflon ablation couple with the MHD system. To treat the rarefaction effects, we modified the wall surface boundary condition with appropriate velocity-slip and temperature-jump conditions. To handle very large density jumps in the micro-PPT simulation, a numerical strategy is introduced to maintain the pressure positive. A high-order discontinuous Galerkin treatment is used in the simulation.

ACKNOWLEDGEMENT

This work was supported by the Computational Mathematics program of AFOSR. Computations were performed at NPACI's and Brown's IBM SP3. We would like to thank Prof. N. Gatsonis and Dr. Sergey Surzikov of WPI for very useful suggestions regarding this work.

References

[1] H. Kamhawi and P.J. Turchi. Design, operation, and investigation of an inductively-driven pulsed plasma thruster. In *34th AIAA/ASME/SAE/ASEE Joint Propulsion Conference Exhibit*, Cleveland, OH, 1998.

[2] P.J.Turch, I.G. Mikelides, P.G. Mikelides, and H. Kamhawi. Optimization of pulsed plasma thrusters for microsatellite propulsion. In *35th AIAA/ASME/SAE/ASEE Joint Propulsion Conference Exhibit*, Los Angeles, CA, 1999.

[3] C.A. Scharlemann, R. Corey, P.G. Mikelides, and P.J. Turchi. Pulsed plasma thrusters variations for improved mission capabilities. In *36th AIAA/ASME/SAE/ASEE Joint Propulsion Conference Exhibit*, Huntsville, Alabama, 2000.

[4] P.G. Mikelides H. Kamhawi, P.J. Turch and I.G. Mikelides. Experimental and theoretical investigation of an inverse-pinch coaxial pulsed plasma thruster. In *36th AIAA/ASME/SAE/ASEE Joint Propulsion Conference Exhibit*, Huntsville, Alabama, 2000.

[5] F.S. Gulczinski, M.J. Dulligan, J.P. Lake, and G.G. Spanjers. Micropropulsion research at afrl. In *36th AIAA/ASME/SAE/ASEE Joint Propulsion Conference Exhibit*, Huntsville, Alabama, 2000.

[6] K.G. Powell. An approximate Riemann solver for magnetohydrodynamics. *Technical Report ICASE Report*, 94:24, 1994.

[7] A.L. Zachary, A. Malagoli, and P. Colella. A higher-order Godunov method for multidimensional ideal magnetohydrodynamics. *SIAM J. Sci. Stat Comp.*, 15:15, 1994.

[8] W. Dai and P.R. Woodward. A simple Riemann solver and high-order Godunov schemes for hyperbolic systems of conservation laws. *Journal of Computational Physics*, 121:51, 1995.

[9] R.E. Peterkin, M.H. Frese, and C.R. Sovinec. Transport magnetic flux in an arbitrary coordinate ALE code. *Journal of Computational Physics*, 140:148, 1998.

[10] O.S. Jones, U. Shumlak, and D.S. Eberhardt. An implicit scheme for nonideal magnetohydrodynamics. *Journal of Computational Physics*, 130:231, 1997.

[11] P. Colella, M. Dorr, and D.D. Wake. A conservative finite difference method for the numerical solution of plasma fluid equations. *Technical Report UCRL-JC-129912*, 1998.

[12] G. Lin and G.E. Karniadakis. A high-order discontinuous galerkin method for modeling micro-pulsed plasma thrusters. In *27th international electric propulsion conference*, Pasadena, CA, 2001.

[13] G.E. Karniadakis and A. Beskok. *Micro Flows: Fundamentals and Simulation.* Springer, 2001.

[14] D.S. Balsara and D. Spicer. Maintaining pressure positivity in magnetohydrodynamic simulations. *Journal of Computational Physics*, 148:133–148, 1999.

[15] S.A. Schaaf and P.I. Chambre. *Flow of rarefied gases.* Princeton, 1961.

[16] P.G. Mikellides and P.J. Turchi. Modeling of late-time ablation in teflon pulsed plasma thrusters. In *32nd AIAA/ASME/SAE/ASEE Joint Propulsion Conference Exhibit*, Buena Vista, FL, 1996.